

# Large On-Off Ratios and Negative Differential Resistance in a Molecular Electronic Device

J. Chen,<sup>1</sup> M. A. Reed,<sup>1\*</sup> A. M. Rawlett,<sup>2</sup> J. M. Tour<sup>2\*</sup>

A molecule containing a nitroamine redox center (2'-amino-4-ethynylphenyl-4'-ethynylphenyl-5'-nitro-1-benzenethiol) was used in the active self-assembled monolayer in an electronic device. Current-voltage measurements of the device exhibited negative differential resistance and an on-off peak-to-valley ratio in excess of 1000:1.

Electron transport studies in molecular-scale systems have recently become possible with the use of advanced microfabrication and self-assembly techniques (1, 2). Investigations of the electronic conduction through conjugated molecules that are end-bound onto surfaces are now possible and have been demonstrated with a scanning tunneling microscope (3), micromachined silicon nanopores (4), and proximal probes (5, 6). Here we report the observation of large reversible switching behavior in an electronic device that uses molecules as the active component.

Electronic measurements were performed in a nanostructure that had a metal top contact, a self-assembled monolayer (SAM) active region, and a metal bottom contact. This nanostructure is similar to one reported previously (4) and is summarized in Fig. 1. The essential feature of the fabrication process is the use of a nanoscale device area, which gives rise to a small number of self-assembled molecules ( $\approx 1000$ ) and also eliminates pinhole and other defect mechanisms that hamper through-monolayer electronic transport measurements. We achieved good control over the device area while also creating intrinsic contact stability. We could produce a large number of devices with acceptable yield, so that statistically significant results could be obtained.

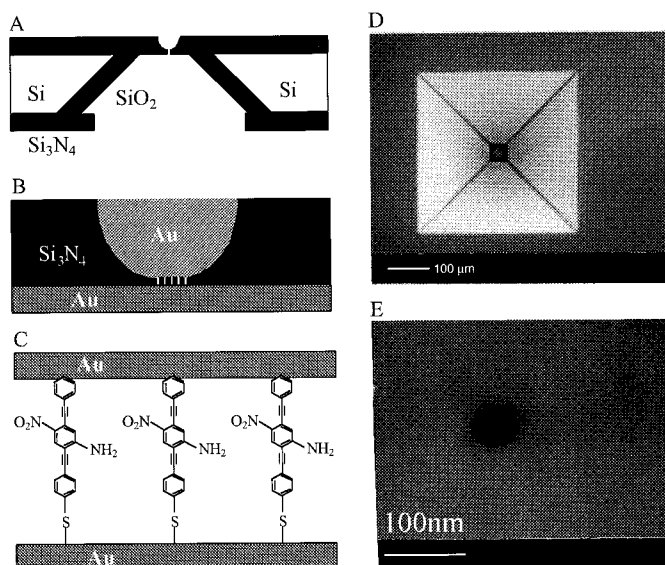
The starting substrate for the device fabrication was a 250- $\mu\text{m}$ -thick double-side polished silicon (100) wafer, on which 50 nm of low-stress  $\text{Si}_3\text{N}_4$  was deposited by low-pressure chemical vapor deposition. On the back surface, the nitride was removed in a square 400  $\mu\text{m}$  by 400  $\mu\text{m}$  by optical lithography and reactive ion etching (RIE). The exposed silicon was etched in an orientation-dependent anisotropic etchant (at 85°C in a 35%

KOH solution) through to the top surface to leave a suspended silicon nitride membrane 40  $\mu\text{m}$  by 40  $\mu\text{m}$ . We then thermally grew 1000 Å of  $\text{SiO}_2$  on the Si sidewalls to improve electrical insulation. A single hole 30 to 50 nm in diameter was made through the membrane by electron beam lithography and RIE (7). Because of the constrained geometry, the RIE rates were substantially reduced so that the far side opening was much smaller than the actual pattern, thereby producing the bowl-shaped geometry of the cross section. A Au contact of 200 nm thickness was evaporated onto the top side of the membrane, which filled the pore with Au. The sample was then immediately transferred into a solution to self-assemble the active electronic component 2'-amino-4-ethynylphenyl-4'-ethynylphenyl-5'-nitro-1-benzenethiolate (1c). This compound was synthesized starting

with 0.5 mM 2'-amino-4-ethynylphenyl-4'-ethynylphenyl-5'-nitro-1-(thioacetyl) benzene (1a) (8). The thioacetyl groups were selectively hydrolyzed with ammonium hydroxide (concentrated aqueous 14.8 M  $\text{NH}_4\text{OH}$ , 5  $\mu\text{l}$  per milligram of 1a) in tetrahydrofuran (THF) to yield the free thiol 2'-amino-4-ethynylphenyl-4'-ethynylphenyl-5'-nitro-1-benzenethiol (1b), which then formed the thiolate (1c) upon exposure to Au after 48 hours (9) under an inert atmosphere of Ar. The sample was then rinsed, quickly loaded into a vacuum chamber, and mounted onto a liquid nitrogen cooling stage for the bottom Au electrode evaporation, in which 200 nm of Au was evaporated at 77 K at a rate of less than 1 Å/s. The devices were then diced into individual chips, bonded onto packaging sockets and loaded into a variable temperature cryostat (Janis), and measured with a HP4145 Semiconductor Parameter Analyzer.

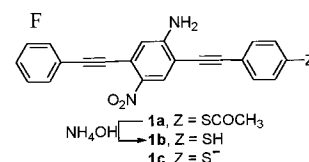
A series of control experiments was performed with alkanethiol-derived SAMs, silicon nitride membranes without pores, and membranes with pores but without molecules. Both the Au-alkanethiolate-Au junctions and the Au-silicon nitride membrane-Au junctions showed current levels at the noise limit of the apparatus ( $< 1$  pA) for both bias polarities at room and low temperatures. The Au-Au junctions gave ohmic current-voltage [ $I(V)$ ] characteristics with very low resistances. A device containing a SAM of conjugated molecules similar to 1c but not bearing the nitroamine functionalities was

**Fig. 1.** Schematics of device fabrication. (A) Cross section of a silicon wafer with a nanopore etched through a suspended silicon nitride membrane. (B) Au-SAM-Au junction in the pore area. (C) Blowup of (B) with 1c sandwiched in the junction. (D) Scanning electron micrograph (SEM) of pyramid Si structure after unisotropic Si etching [that is, the bottom view of (A)]. (E) SEM of an etched nanopore through the silicon nitride membrane. (F) The active molecular compound 1c and its precursors the free thiol 1b and the thiol-protected system 1a.



<sup>1</sup>Departments of Electrical Engineering, Applied Physics, and Physics, Yale University, Post Office Box 208284, New Haven, CT 06520, USA. <sup>2</sup>Department of Chemistry and Center for Nanoscale Science and Technology, Rice University, Mail Stop 222, 6100 Main Street, Houston, TX 77005, USA.

\*To whom correspondence should be addressed.



## REPORTS

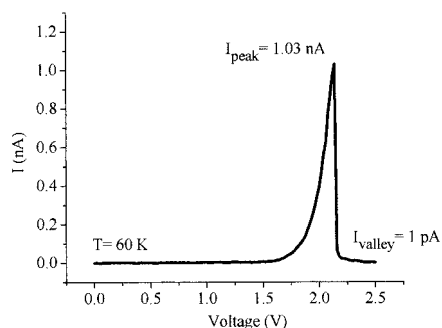


**Fig. 2.**  $I(V)$  characteristics of a Au-(2'-amino-4-ethynylphenyl-4'-ethynylphenyl-5'-nitro-1-benzenethiolate)-Au device at 60 K. The peak current density is  $\sim 50$  A/cm<sup>2</sup>, the NDR is  $\sim -400$   $\mu\text{ohm} \cdot \text{cm}^2$ , and the PVR is 1030:1.

fabricated and measured in nearly identical conditions (10) and did not exhibit any negative differential resistance (NDR) behavior.

Typical  $I(V)$  characteristics of a Au-(1c)-Au device at 60 K are shown in Fig. 2. Positive bias corresponds to hole injection from the chemisorbed thiol-Au contact and electron injection from the evaporated contact. The peak current density for this device was  $>53$  A/cm<sup>2</sup>, the NDR was  $<-380$   $\mu\text{ohm} \cdot \text{cm}^2$ , and the peak-to-valley ratio (PVR) was 1030:1. Unlike previous devices that also used molecules to form the active region (11), this device exhibits a robust and large NDR. Some device-to-device variations of peak voltage position

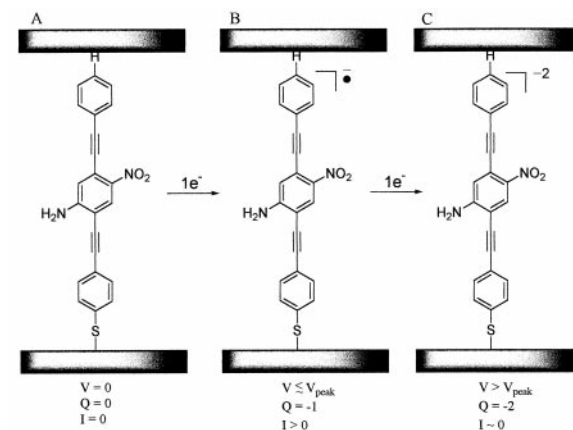


**Fig. 4.** Potential mechanism for the NDR effect. As voltage is applied, the molecules in the SAM (A) undergo a one-electron reduction to form the radical anion (B) that provides a conductive state. Further increase of the voltage causes another one-electron reduction to form the dianion insulating state (C). Q is the charge.

( $\sim \times 2$ ) and peak current ( $\sim \times 4$ ) were observed (7). The  $I(V)$  curve was fully reversible upon change in bias sweep direction; for a given device, small fluctuations ( $\sim 1\%$  in voltage peak position and  $\sim 6\%$  in peak current) were observed with consecutive positive and negative sweeps but could be attributed to temperature fluctuations of  $\sim 2$  K (within the experimental thermal stability). The performance exceeds that observed in typical solid-state quantum well resonant tunneling heterostructures (12–15). In addition to the obvious size advantages for scaling, the intrinsic device characteristics (that is, the valley current shutoff) may be superior to those of solid-state devices. The intrinsic PVR of the molecule may be considerably greater than that reported here because the valley currents observed (on the order of picoamperes) are comparable to typical leakage currents in the silicon nitride. All of the devices examined exhibited peak voltage position and current magnitude shifts with temperature such as those shown in Fig. 3.

A candidate mechanism for the NDR is a two-step reduction process that modifies charge transport through the molecule, as illustrated in Fig. 4. As the voltage is increased, the molecule initially undergoes a one-electron reduction, thereby supplying a charge carrier for electron flow through the system (although the nitro moiety is the most electron-withdrawing group in the molecule, the charge is probably dispersed throughout the entire molecule). A further increase in voltage causes a second electron reduction with subsequent blocking of the current. The width of the  $I(V)$  peak ( $\sim 0.7$  V) correlates well with the difference between the one-electron and two-electron peak reduction potentials [ $E_{p2} - E_{p1} = \Delta E_p = 0.63$  V and  $0.68$  V for **1** with  $z$  (the end group as in Fig. 1F) =  $\text{SCH}_3$  and  $Z = \text{H}$ , respectively] (16). The NDR behavior was absent in the control molecule (no amine or nitro moieties) (10), and no electrochemical reduction peaks were observed over the corresponding voltage

range. Theory to explain the temperature dependencies and future experimental work to examine frequency and optical response should elucidate the transport mechanisms that would further permit engineering of device performance for room-temperature operation (17). The NDR observation cannot be explained by the Coulomb blockade of interstitial metal particles, because two-terminal localized state transport gives rise to current steps (18) and not switching behavior.

Two-terminal NDR devices have numerous device applications, including high-frequency oscillators (19), mixers, multipliers, logic (20), and analog-to-digital converters (21); and three-terminal devices incorporating NDR give rise to novel compact circuits (22, 23). The use of NDR SAMs could implement these applications.

## References and Notes

1. A. Aviram and M. Ratner, Eds., *Molecular Electronics: Science and Technology* (Annals of the New York Academy of Sciences, New York, 1998).
2. M. C. Petty, M. R. Bryce, D. Bloor, Eds., *An Introduction to Molecular Electronics* (Oxford Univ. Press, New York, 1995).
3. L. A. Bumm *et al.*, *Science* **271**, 1705 (1996).
4. C. Zhou *et al.*, *Appl. Phys. Lett.* **71**, 611 (1997).
5. M. A. Reed *et al.*, *Science* **278**, 252 (1997).
6. C. Kergueris *et al.*, *Phys. Rev. B* **59**, 12505 (1999).
7. Device-to-device current fluctuations can be attributed to fluctuations in pore diameter size.
8. The starting compound (**1a**) was prepared by sequential Pd/Cu-catalyzed coupling of 2,5-dibromo-4-nitroacetanilide with phenylacetylene and 4-ethynyl-(thioacetyl)benzene.
9. J. M. Tour *et al.*, *J. Am. Chem. Soc.* **117**, 9529 (1995).
10. C. Zhou, thesis, Yale University (1999).
11. Weak room-temperature NDR has previously been reported [M. A. Reed, *Proc. IEEE* **87**, 652 (1999)].
12. J. H. Smet, T. P. E. Broekaert, C. G. Fonstad, *J. Appl. Phys.* **71**, 2475 (1992).
13. J. R. Söderström, D. H. Chow, T. C. McGill, *J. Appl. Phys.* **66**, 5106 (1989).
14. J. Day *et al.*, *J. Appl. Phys.* **73**, 1542 (1993).
15. H. H. Tsai *et al.*, *IEEE Electron. Device Lett.* **15**, 357 (1993).
16. The case where  $Z = \text{SH}$  was avoided because of anomalies that could be caused through electrochemical disulfide formation and cleavage events.
17. Since submission of the manuscript, room-temperature NDR (PVR = 1.5:1) has been observed in a similar molecule.
18. M. R. Deshpande *et al.*, *Phys. Rev. Lett.* **76**, 1328 (1996).

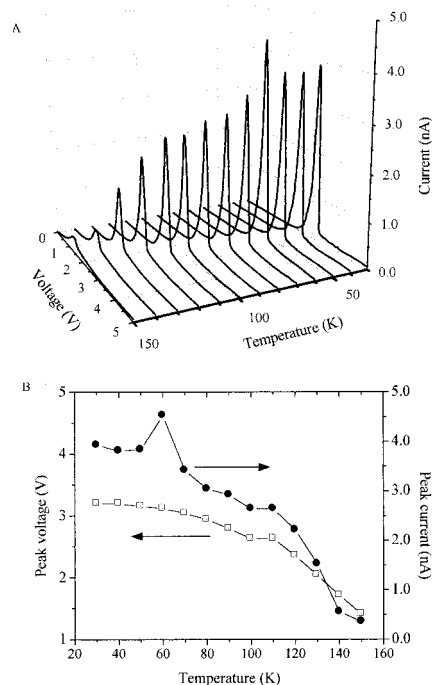


**Fig. 3.** (A)  $I(V,T)$  characteristics ( $T$  is temperature) of a Au-(2'-amino-4-ethynylphenyl-4'-ethynylphenyl-5'-nitro-1-benzenethiolate)-Au device. (B) Peak voltages and currents of  $I(V)$  curves at different temperatures.

19. E. R. Brown *et al.*, *Appl. Phys. Lett.* **58**, 229 (1991).  
 20. R. H. Mathews *et al.*, *Proc. IEEE* **87**, 596 (1999).  
 21. T. P. E. Broekaert *et al.*, *IEEE J. Solid State Circ.* **33**, 1342 (1998).  
 22. C. Seabaugh and M. A. Reed, in *Heterostructures and*

*Quantum Devices*, N. G. Einspruch and W. R. Frensley, Eds. (Academic Press, Orlando, FL, 1994), pp. 351–383.  
 23. J. Huber *et al.*, *IEEE Trans. Electron. Devices* **44**, 2149 (1997).

24. Supported by the Defense Advanced Research Projects Agency through the Office of Naval Research under grant N00014-99-1-0406.

22 July 1999; accepted 22 October 1999

# Feedback Connections to the Lateral Geniculate Nucleus and Cortical Response Properties

Penelope C. Murphy,<sup>1,2\*</sup> Simon G. Duckett,<sup>1</sup> Adam M. Sillito<sup>2</sup>

The cerebral cortex receives sensory input from the periphery by means of thalamic relay nuclei, but the flow of information goes both ways. Each cortical area sends a reciprocal projection back to the thalamus. In the visual system, the synaptic relations that govern the influence of thalamic afferents on orientation selectivity in the cortex have been studied extensively. It now appears that the connectivity of the corticofugal feedback pathway is also fundamentally linked to the orientation preference of the cortical cells involved.

An abiding challenge for vision research is to determine the role of the massive feedback pathway from the visual cortex to the dorsal lateral geniculate nucleus (dLGN), the specific visual relay nucleus in the thalamus. Axons feeding back from cortical areas 17 and 18 contribute substantially more synapses to the geniculate neuropil than any other source of input, including the retina (1–3). It has been suggested that they might simply provide a nonspecific facilitation of the thalamic circuit, but growing evidence (4, 5) favors a more active role in visual processing. Cells in this pathway are selective for both the orientation and the direction of movement of a visual stimulus (6, 7), and their influence has been shown to reflect both properties (8–10). Geniculate cells respond to stimuli at any orientation (11), but feedback makes them sensitive to orientation context (8). Feedback also influences the level of synchronization of cells responding to the presence of a single elongate stimulus, as distinct from those responding to individual, more localized stimuli (12). It has been proposed that this might enhance the salience of such contours within a visual image, which in turn might influence both the generation and expression of orientation selectivity at the cortical level.

Corticofugal axons have large arborizations, which can encompass substantial regions of the geniculate retinotopic map (4). Given entirely random connections, a cortical

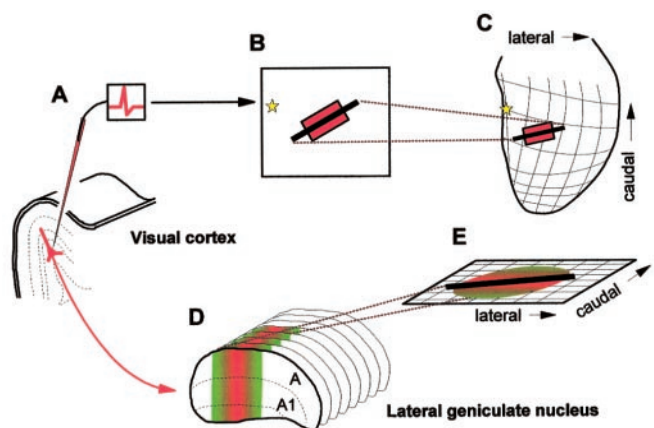
cell responding to one contour might be expected to synchronize geniculate cells responding to widespread and entirely unrelated aspects of a complex natural scene. Any selectivity would have to arise from precise temporal links between the ascending and descending inputs. Alternatively, the effectiveness of the system could be enhanced by a more specific pattern of connections that link the oriented cortical cells with the array of geniculate afferents from which they receive input. Corticofugal axons are for the most part extremely sparse, which suggests that they exert only a weak influence over the majority of their postsynaptic targets. However, they show restricted regions of greatly increased bouton density (4), within which they ought to exert a more effective influence. An obvious question is whether there is

any relation between these anatomical “hot spots” and the representation of visual space in the dLGN.

We stained 25 single corticofugal axons, 13 from area 17 and 12 from area 18 of the cat visual cortex (4, 13, 14). The orientation preferences of the cells of origin were determined before staining, either by direct recording of intracellularly stained cells or by mapping representative cells from the same orientation columns (15, 16). Stained axons were identified and reconstructed from serial sections, and the distribution of their synaptic boutons within the A layers of the dLGN was quantified with respect to the geniculate retinotopic map (17) (Fig. 1, A, D, and E).

The boutons from individual axons are sparsely distributed over a wide region of the dLGN; the average range spread from  $755 \pm 85 \mu\text{m}$  to  $940 \pm 130 \mu\text{m}$  rostrocaudal, and from  $1020 \pm 75 \mu\text{m}$  to  $1240 \pm 100 \mu\text{m}$  mediolateral, for areas 17 and 18, respectively. This delineates an area many times the size of the geniculate representation of the corticofugal cell receptive fields (Fig. 2, B to D). Within this area, however, are regions of much higher bouton density, which more closely match the receptive field dimensions. In some cases, a single discrete peak is formed (Fig. 3, C and E) and in others, multiple peaks (Fig. 3, B, D, and F). In either case, these zones are almost invariably elongate. To quantify the degree of elongation, only regions with a greater than half-maximal bouton count were selected. Under these cir-

**Fig. 1** Experimental protocol. (A) Cells in visual cortical areas 17 and 18 were recorded, mapped, and then labeled with biocytin (4, 13). (B and C) Their receptive fields (B) were superimposed on the geniculate retinotopic map of visual space (C). This map (18) is highly nonlinear. Therefore, key points from each field were accurately located with respect to the grid of iso-azimuth and iso-elevation lines, and the field’s axis of orientation was redrawn with correction for local scale. The angle of this line was measured with respect to the mediolateral axis of the map. Stars represent the area centralis; rectangle, minimum discharge zone of cortical receptive field; thick bar, preferred orientation. (D and E) Single axons were reconstructed from the histochemically treated sections, and the distributions of their boutons were quantified in three dimensions (17) and then analyzed with respect to their relation to the geniculate representation of visual space.



<sup>1</sup>Department of Physiology, St. George’s Hospital Medical School, Tooting, London SW17 0RE, UK. <sup>2</sup>Department of Visual Science, Institute of Ophthalmology, University College London, Bath Street, London EC1V 9EL, UK.

\*To whom correspondence should be addressed. E-mail: p.murphy@sghms.ac.uk